Dynamics of reactions O (D 1) + C 6 H 6 and C 6 D 6

Hui-Fen Chen, Chi-Wei Liang, Jim J. Lin, Yuan-Pern Lee, J. F. Ogilvie, Z. F. Xu, and M. C. Lin

Citation: The Journal of Chemical Physics **129**, 174303 (2008); doi: 10.1063/1.2994734
View online: http://dx.doi.org/10.1063/1.2994734
View Table of Contents: http://scitation.aip.org/content/aip/journal/jcp/129/17?ver=pdfcov
Published by the AIP Publishing

Dynamics of reactions $O(^1D)+C_6H_6$ and C_6D_6

Hui-Fen Chen,[1] Chi-Wei Liang,[2] Jim J. Lin,[3,4,a)] Yuan-Pern Lee,[3,4,a)] J. F. Ogilvie,[5] Z. F. Xu,[6] and M. C. Lin[3,6,a)]
[1]*Department of Chemistry, National Tsing Hua University, Hsinchu 30013, Taiwan*
[2]*Department of Chemistry, National Taiwan University, Taipei 10617, Taiwan*
[3]*Department of Applied Chemistry and Institute of Molecular Science, National Chiao Tung University, Hsinchu 30010, Taiwan*
[4]*Institute of Atomic and Molecular Sciences, Academia Sinica, Taipei 10617, Taiwan*
[5]*Escuela de Qumica, Universidad de Costa Rica, Ciudad Universitaria Rodrigo Facio, San Pedro de Montes de Oca, San Jose 2060, Costa Rica*
[6]*Department of Chemistry, Emory University, Atlanta, Georgia 30322, USA*

(Received 8 July 2008; accepted 15 September 2008; published online 4 November 2008)

The reaction between $O(^1D)$ and C_6H_6 (or C_6D_6) was investigated with crossed-molecular-beam reactive scattering and time-resolved Fourier-transform infrared spectroscopy. From the crossed-molecular-beam experiments, four product channels were identified. The major channel is the formation of three fragments $CO+C_5H_5+H$; the channels for formation of C_5H_6+CO and C_6H_5O+H from $O(^1D)+C_6H_6$ and $OD+C_6D_5$ from $O(^1D)+C_6D_6$ are minor. The angular distributions for the formation of CO and H indicate a mechanism involving a long-lived collision complex. Rotationally resolved infrared emission spectra of CO ($1 \le v \le 6$) and OH ($1 \le v \le 3$) were recorded with a step-scan Fourier-transform spectrometer. At the earliest applicable period (0–5 μs), CO shows a rotational distribution corresponding to a temperature of ~1480 K for $v=1$ and 920–700 K for $v=2-6$, indicating possible involvement of two reaction channels; the vibrational distribution of CO corresponds to a temperature of ~5800 K. OH shows a rotational distribution corresponding to a temperature of ~650 K for $v=1-3$ and a vibrational temperature of ~4830 K. The branching ratio of $[CO]/[OH]=2.1\pm0.4$ for $O(^1D)+C_6H_6$ and $[CO]/[OD]>2.9$ for $O(^1D)+C_6D_6$ is consistent with the expectation for an abstraction reaction. The mechanism of the reaction may be understood from considering the energetics of the intermediate species and transition states calculated at the G2M(CC5) level of theory for the $O(^1D)+C_6H_6$ reaction. The experimentally observed branching ratios and deuterium isotope effect are consistent with those predicted from calculations. © *2008 American Institute of Physics*. [DOI: 10.1063/1.2994734]

I. INTRODUCTION

The reactions of singlet oxygen atoms $O(^1D)$ are important in atmospheric chemistry because $O(^1D)$ is highly reactive toward small molecules in the atmosphere. Reactions of $O(^1D)$ with hydrogen,[1–3] water,[4–8] methane,[9–15] and higher saturated hydrocarbons[16–23] have been extensively investigated. Previous experiments on the dynamics of formation of OH from reactions of $O(^1D)$ with saturated hydrocarbons indicated two possible paths: insertion of $O(^1D)$ and direct abstraction of H.[16,24–26] Several theoretical investigations[16–19,27–30] on the reaction mechanisms of $O(^1D)+CH_4$, C_2H_6, and c-C_3H_6 supported the reported experimental observations.

In contrast, reactions between $O(^1D)$ and unsaturated hydrocarbons have been investigated to a less extent.[31–35] Sato and Cvetanović[31] and Kajimoto *et al.*[33] reported the formation of both enols, via an insertion of $O(^1D)$ into a C–H bond, and epoxides, via an addition of $O(^1D)$ into a C=C double bond, in these reactions. Based on the observed relative product yields, Kajimoto *et al.*[33] concluded that the epoxide channel occurs more readily than the enol channel. Honma[34] employed laser-induced fluorescence (LIF) to determine the distributions of rotational and vibrational states of OH produced from the reaction of $O(^1D)$ with C_2H_4 under flow conditions at low pressure and reported bimodal rotational distributions of OH ($v=0$ and 1). Gonzalez *et al.*[35] reported bimodal rotational distributions for OH ($v=0$ and 3) and unimodal ones for OH ($v=1$ and 2) determined with LIF; they suggested that, in contrast to what was proposed by Kajimoto *et al.*,[33] the reaction evolves preferentially via insertion of $O(^1D)$ into the C−H bond, yielding internally cold OH through slow decomposition of an enol-type intermediate and internally excited OH by rapid elimination before the relaxation of the internal energy of the intermediate. They proposed also that the production of rotationally cold but vibrationally hot OH ($v=3$) occurred via an abstraction channel.

Several experimental[36–40] and theoretical[41,42] investigations on reactions of $O(^3P)$ with aromatic compounds have been reported. Sibener *et al.*[36] investigated the reaction of $O(^3P)+C_6H_6$ with crossed-molecular beams and concluded that the initially formed triplet biradical C_6H_6O either de-

a)Authors to whom correspondence should be addressed. Electronic addresses: jimlin@gate.sinica.edu.tw, yplee@mail.nctu.edu.tw, and chemmcl@emory.edu.

composes to eliminate a hydrogen atom [reaction (1)] or becomes stabilized likely via a nonradiative transition to the ground state (S_0) manifold of phenol [reaction (2)],

$$O(^3P) + C_6H_6 \rightarrow C_6H_5O + H, \quad (1)$$

$$O(^3P) + C_6H_6 \rightarrow C_6H_5OH, \quad (2)$$

$$O(^3P) + C_6H_6 \rightarrow C_5H_6 + CO, \quad (3)$$

$$O(^3P) + C_6H_6 \rightarrow C_6H_5 + OH. \quad (4)$$

Barry *et al.*[38] investigated the reaction of a crossed-molecular beam of $O(^3P)+C_6H_6$ at a collision energy of 16.5 kcal mol^{-1} and reported little (0.8 kcal mol^{-1}) rotational excitation of the OH product detected by LIF; the results indicate that the reaction might proceed directly via an O−H−C collinear transition structure. Theoretical calculations[41,42] indicated that reactions (1) and (2) are major channels, whereas reaction (4) becomes important at high temperatures with an estimated branching ratio of 50% at 2000 K. Reaction (3) was predicted to be a minor channel with a yield of <5% even under flame conditions.

There is no report on the kinetics or dynamics of the reaction $O(^1D)+C_6H_6$. On the basis of the present understanding of reactions of $O(^3P)$ with benzene and of $O(^3P)$ and $O(^1D)$ with alkanes and alkenes, the reaction of $O(^1D)$ with benzene is expected to occur more readily than of $O(^3P)$ with benzene and to produce both singlet phenol (C_6H_5OH) and benzene epoxide ($O<C_6H_6$) as intermediates, in which "O<" in the formula indicates an epoxide structure. The mechanisms established previously for the thermal and photolytic decomposition of phenol might also assist us in understanding the reaction mechanism of $O(^1D)+C_6H_6$.[43,44]

In this work, we have investigated the reactions of $O(^1D)+C_6H_6$ and C_6D_6 through the determination of translational energy distributions and the branching ratios of various channels,

$$O(^1D) + C_6H_6 \rightarrow CO + C_5H_6, \quad (5a)$$

$$O(^1D) + C_6H_6 \rightarrow CO + C_5H_6^* \rightarrow CO + C_5H_5 + H, \quad (5b)$$

$$O(^1D) + C_6H_6 \rightarrow H + C_6H_5O, \quad (6a)$$

$$O(^1D) + C_6H_6 \rightarrow H + C_6H_5O^* \rightarrow H + C_5H_5 + CO, \quad (6b)$$

$$O(^1D) + C_6H_6 \rightarrow OH + C_6H_5, \quad (7)$$

with crossed-molecular beams and by measurements of internal-state distributions and branching ratios of CO and OH with time-resolved Fourier-transform infrared (FTIR) emission.[45,46] Reactions (5a) and (5b) produce CO as a primary product; some C_5H_6 are stable, listed as reaction (5a), and some C_5H_6 might have enough internal energy (indicated as $C_5H_6^*$) to dissociate further to C_5H_5+H, listed as reaction (5b). Similarly, reaction (6a) indicates the production of H and stable C_6H_5O, whereas reaction (6b) indicates that energetic $C_6H_5O^*$ further decomposes to yield C_5H_5+CO. The products of reactions (5b) and (6b) are identical, although they are dynamically produced from two distinct reaction paths. We have also performed electronic structure calculations to predict the energetics of the reaction intermediates and transition states on the potential-energy surfaces (PES) of the O+benzene reaction and used them to predict, with statistical rate calculations, the rate coefficients and branching ratios.

II. EXPERIMENTS

A. Crossed-molecular-beam experiments

As most features of the crossed-molecular-beam apparatus have been described previously,[47] only the relevant part of the experimental setup is described here. An atomic beam of $O(^1D)$ was generated upon laser photolysis at 157.6 nm of a skimmed molecular beam of O_2,[48]

$$O_2 + h\nu(157.6 \text{ nm}) \rightarrow O(^1D) + O(^3P). \quad (8)$$

The output of a F_2 excimer laser (Lambda Physik, LPX 210i, F_2 version, 30–50 mJ pulse^{-1}) was focused with a special spherical-cylindrical MgF_2 lens to a spot size of 3×3 mm^2. Under such conditions, $O(^3P)$ atoms were generated also in approximately equal proportions. The $O(^1D)$ atomic beam had a narrow velocity distribution (<2%) and an angular divergence of about ±4° [full width at half maximum (FWHM)]. The $O(^1D/^3P)$ atomic beam has a mean speed of 2290 m s^{-1}.

Even though the reactivity of an $O(^3P)$ atom toward benzene is expected to be smaller than that of $O(^1D)$,[49,50] the contribution from $O(^3P)$ was carefully examined. The output of an ArF excimer laser (Lambda Physik, LPX 210i, 20–25 mJ pulse^{-1}), focused with two cylindrical fused-silica lenses to a spot size of 4×4 mm^2, photodissociated a molecular beam of SO_2 to generate a beam of $O(^3P)$ with negligible $O(^1D)$,

$$SO_2 + h\nu(193 \text{ nm}) \rightarrow SO(^3\Sigma^-) + O(^3P). \quad (9)$$

Because diverse vibration-rotational states of SO photofragments are populated upon photolysis of SO_2,[51] the atomic beam of $O(^3P)$ had a broad velocity distribution (~33%, FWHM) with an angular divergence of about ±6° (FWHM). Since the velocity distribution of the $O(^3P)$ atom was intrinsically broad, the SO_2 beam was not skimmed to enhance the intensity. The mean speed of the $O(^3P)$ atomic beam was about 2300 m s^{-1}. To achieve similar conditions for comparison, the molecular beam of O_2 was also not skimmed in some experiments. S $^{18}O_2$ (97% ^{18}O), synthesized on burning sulfur powder under $^{18}O_2$ gas, was employed to produce $^{18}O(^3P)$.

A molecular beam of benzene was generated on expanding a premixed sample (2% in Ne) through a pulsed Even-Lavie valve[52] with its head heated to 488 K to diminish formation of clusters. This valve produces a benzene pulse with width of ~40 μs at the interaction region, hence diminishing significantly the effusive background gases from the beam source. A sharp-edged skimmer (Beam Dynamics, diameter of 2 mm) served to define the angular divergence of about $\pm 1.8°$. Perdeuterated benzene (C_6D_6, isotopic purity >99.95%, ACROS) was used in D-isotopic experiments. The mean speed of the benzene beam was 1050 m s^{-1} with a distribution of 5%.

The two reactant beams crossed each other at 90°; the collision energy was tuned to ~10 kcal mol^{-1} upon adjusting the velocity of the O atomic beam. Products scattered from the reaction center traveled 24 cm before being detected with a time-resolved quadrupole mass filter. The housing of the electron-impact ionizer of the mass filter is differentially pumped in three sections to 10^{-12} Torr so that the background signal from residual gases and scattered gas is diminished. Velocity distributions of the product were derived from the time-of-flight (TOF) spectra of the nascent products, recorded with a multichannel scaler (EG&G, Turbo MCS). The angular distribution of products was measured on rotating the detector. A computer program employs trial distributions of translational energy $P(E_T)$ and angular dispersion $P(\theta)$ of products in the center-of-mass (CM) frame to simulate the TOF spectra in the laboratory frame using forward convolution.[53] $P(E_T)$ and $P(\theta)$ were adjusted iteratively until a satisfactory fit to the experimental TOF spectra and angular distribution was attained. Instrumental functions used in the program were determined from calibration experiments, including photolysis of O_2 at 157.6 nm and $O(^1D)$+Xe quenching/elastic scattering.

B. Time-resolved IR emission experiments

The apparatus employed to obtain step-scan time-resolved Fourier-transform spectra (TR-FTS) has been described previously;[54–56] only a summary is given here. A telescope mildly focused the photolysis beam from a KrF laser (248 nm) to an area of ~6×22 mm^2 at the reaction center to yield a fluence of ~50 mJ cm^{-2}. Filters passing either 1700–2800 cm^{-1} (for the detection of CO) or 2840–4000 cm^{-1} (for the detection of OH) were employed to minimize the number of scan steps. The transient signal from an InSb detector with a rise time of 0.7 μs was preamplified with a gain factor of 10^5 V A^{-1} (EG&G Judson, PA9–50, 1.5 MHz bandwidth), followed by further amplification with a factor of 500 (bandwidth of 1 MHz) before being digitized with an internal data-acquisition board (16 bits) at a resolution of 5 μs. Data were typically averaged over 60 laser pulses at each scan step; 2508 or 4881 scan steps were performed to yield an interferogram resulting in a spectrum with resolution of 1.0 or 0.3 cm^{-1} for OH and CO detection, respectively. To improve the signal to noise ratio (S/N) of the spectrum, we averaged six sets of time-resolved spectra under the same experimental conditions to yield satisfactory spectra. The temporal response function of the instrument was determined with a pulsed IR laser beam, as described previously.[57]

Ozone (O_3) and C_6H_6 were injected into the reaction chamber separately; to decrease the collisional quenching of CO and OH, a minimal pressure yielding acceptable signals was used: $P_{O_3}=0.072-0.097$ Torr and $P_{C_6H_6}=0.020-0.092$ Torr. Flow rates were $F_{O_3}=1.7-2.4$ SCCM and $F_{C_6H_6}=0.4-2.4$ SCCM; SCCM denotes cubic centimeter per minute under standard conditions (273 K and 760 Torr). A large fraction (~60%) of O_3 was dissociated upon irradiation at 248 nm based on the reported absorption cross section of 1.5×10^{-17} cm^2 $molecule^{-1}$ for O_3 at 248 nm.[58] The depletion of O_3 after each laser pulse was modest, as was confirmed by the negligible variation in the signal when we decreased the repetition rate of the photolysis laser from 19 to 12 Hz.

C_6H_6 (Fluka, ≥99.5%) was used without purification except for degassing at 77 K. O_3 was produced from O_2 (Scott Specialty Gases, 99.995%) with an ozone generator (Polymetrics, model T-408), stored over silica gel at 196 K, and eluted from the trap with a small flow of He (Scott Specialty Gases, 99.999%). The partial pressure of O_3 was determined from the absorption of Hg emission at 254 nm in a cell with length of 7.0 cm; the cross section for absorption of O_3 at 254 nm was taken to be 1.15×10^{-17} cm^2.[59]

III. COMPUTATIONAL METHODS

The potential-energy diagram for the reaction system $O(^1D)+C_6H_6$ is extended from those established previously on the thermal decomposition[43] and the photofragmentation[44] of C_6H_5OH based on energies predicted at the highest level of the modified Gaussian-2 method, G2M(CC5).[60] In the G2M calculation, the geometries of reaction intermediates and transition states on the ground electronic surface of C_6H_5OH were optimized with the GAUSSIAN 03 program[61] at the B3LYP/6-311G(d,p) level of theory.[62,63]

Calculations of rate coefficients were performed with the VARIFLEX program[64] based on the microcanonical Rice–Ramsperger–Kassel–Marcus (RRKM) theory and variational transition-state theory[65–70] with corrections for Eckart tunneling[71] and multiwell reflection of the reaction flux.[72] The energy increment was fixed at 10 cm^{-1} in all calculations of sums of states and densities of states that were performed using the modified Beyer–Swinehart algorithm.[73] The component rates were evaluated at the E/J-resolved level and the pressure dependence was treated with calculations based on a one-dimensional master equation using the Boltzmann probability of the reaction complex for the J-distribution. A simple exponential quenching model was employed to calculate the coefficients of collision energy transfer.[74] An average step size of 120 cm^{-1} for energy transfer per collision $\langle \Delta E\rangle_{down}$ was employed for the He buffer gas. The Lennard-Jones (LJ) parameters of buffer gases ($\varepsilon/k_B=10.2$ K and $\sigma=2.56$ Å for He) and complex ($\varepsilon/k_B=450$ K and $\sigma=4.50$ Å, the same as C_6H_5OH) were taken from the literature.[75] For a barrierless association

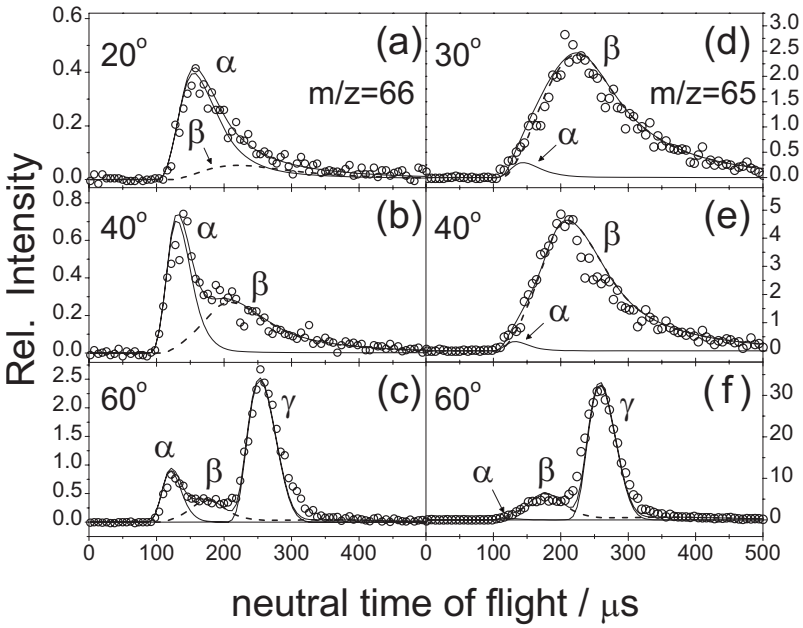

FIG. 1. Representative TOF spectra in the crossed-beam experiment with $O(^1D)+C_6H_6$ at collision energy of 10 kcal mol^{-1} for mass 66 [panels (a)–(c)] and mass 65 [(d)–(f)] at selected laboratory angles. The ordinate scales vary. Three components α, β, and γ are discussed in text.

or decomposition, a fitted Morse function, $V(R)=D_e\{1-\exp[-\beta(R-R_e)]\}^2$, was used in conjunction with an anisotropic potential function to represent the minimum-energy path (MEP) for variational calculations of rate coefficients.

IV. RESULTS

A. Distribution of product translational energy in crossed beams of $O(^1D)+C_6H_6$

Because both $O(^1D)$ and $O(^3P)$ atoms react with C_6H_6, one important issue in this experimental investigation is to distinguish their individual contribution. As the photolyzed O_2 beam yields $O(^1D)$ and $O(^3P)$ atoms in equal proportions, we need another O atom source which provides a different ratio of these two atomic states in order to sort out the individual contributions. Photolysis of SO_2 at 193 nm produces O atoms in its ^3P state; the photon energy is insufficient to produce any $O(^1D)$ atom within the one-photon limit. With the photolyzed SO_2 source, we found that the reaction $O(^3P)+C_6H_6$ produced C_6H_6O [reaction (2)] and $H+C_6H_5O$ [reaction (1)] but no detectable CO, C_5H_6, or C_5H_5 products, consistent with the previous results of crossed-molecular beam using a discharge source.[36] The contribution of the $O(^1D)+C_6H_6$ reaction can then be obtained by subtracting the $O(^3P)$ contribution obtained with the photolyzed SO_2 beam from the results obtained with the photolyzed O_2 beam. We deliberately tuned the velocities of both O atom sources to be similar and quantified their relative intensities with the 70 eV electron-impact ionizer by assuming that the ionization cross sections of $O(^1D)$ and $O(^3P)$ are about equal.

Although reactions (1) and (6a) yield the same C_6H_5O+H products, we found that the reactivity of $O(^1D)$ is at least five times that of $O(^3P)$ for the formation of C_6H_5O. Therefore, the error from this subtraction process is small for reaction (6a). Furthermore, the C_6H_6O product from reaction (2) is unique for having a zero recoil velocity and hence, can be easily separated from the products of the $O(^1D)+C_6H_6$ reaction. The CO formation channels from the $O(^1D)+C_6H_6$ reaction is unaffected by the $O(^3P)+C_6H_6$ reaction due to its negligible contribution. In the following, we focus our discussions on the data which have been adequately corrected to represent the products from the $O(^1D)+C_6H_6$ reaction.

As formation of $CO+C_5H_6$ is expected from the $O(^1D)+C_6H_6$ reaction,[42–44] we first searched for a signal of C_5H_6. TOF spectra of mass 66 at three representative laboratory angles are shown in frames (a)−(c) of Fig. 1; in these spectra three components are observed [Fig. 1(c)]. The two slower components (designated as β and γ) arise from the naturally abundant ^{13}C-isotopic $C_5H_5^+$. As the signals at mass 65 ($C_5H_5^+$) are much larger than those at mass 66, this $^{13}C^{12}C_4H_5^+$ signal has intensity comparable to that of $^{12}C_5H_6^+$. After subtraction of the contribution from the ^{13}C isotope, only the most rapid component (designated as α) remains, which we adopted to be due to channel (5a). To ensure the validity of the subtraction for the ^{13}C-species, we also performed the experiment $O(^1D)+C_6D_6$, in which there is no such isotopic contamination. The distribution of kinetic energy at mass 72 ($C_5D_6^+$) is nearly identical to that of the rapid component at mass 66 in the experiment of $O(^1D)+C_6H_6$.

Frames (d)−(f) of Fig. 1 show the signals at mass 65 observed in the experiments of $O(^1D)+C_6H_6$. The signal might arise from three possible sources: (1) reactions (5b) and (6b) to produce $CO+C_5H_5+H$, (2) the daughter ion of C_5H_6 that was produced from reaction (5a), and (3) the daughter ion of C_6H_5O that was produced from reaction (6a).

Figure 2 shows the Newton diagram for the observed products of reactions (5a), (6a), (5b), and (6b). The Newton circle of C_6H_5O is expected to be small because the H atom coproduct carries away almost 99% of the total translational energy. The component γ at mass 65 [Fig. 1(f)] has almost identical TOF and angular distributions to those for the signal at mass 93 ($C_6H_5O^+$). A comparison of their angular distributions in the laboratory frame is shown in Fig. 3. The

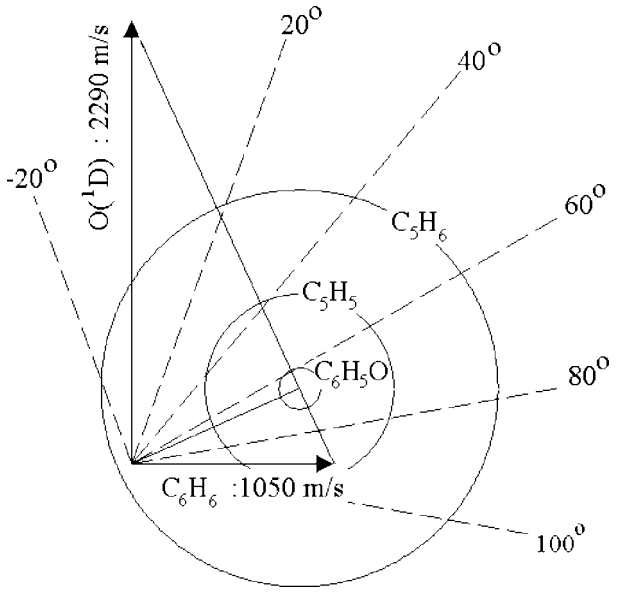

FIG. 2. Newton diagram for the crossed-beam experiment with O(^1D)+C_6H_6 at collision energy of 10 kcal mol^{-1}. Three representative Newton circles are for C_5H_6 product of channel (5a) at $E_{T,\text{peak}}$=28 kcal mol^{-1}, C_5H_5 product of channels (5b) and (6b) at $E_{T,\text{peak}}$=6 kcal mol^{-1}, and C_6H_5O product of channel (6a) at $E_{T,\text{peak}}$=12 kcal mol^{-1}.

similarity of angular distributions and their TOF spectra at masses 65 and 93 leads us to conclude that the γ component at mass 65 represents a daughter ion of C_6H_5O.

The second possible source of mass 65, the daughter ion of C_5H_6, can contribute only slightly to the signal because the TOF spectra of those two masses are disparate. Here only a minor portion of signals at mass 65 [designated as α in Figs. 1(d)–1(f)] is attributed to the daughter ion of C_5H_6. The relative contribution of component α is obtainable from the momentum-matched CO coproduct (see discussion below). After considering two of the three possible sources for the observed $C_5H_5^+$ TOF spectra, the most reasonable assignment for the remaining β component is a product from channels (5b) and (6b).

According to quantum-chemical calculations (discussed below), 1,3-cyclopentadiene is the most likely isomer for the C_5H_6 product. The ionization energy of this species is 8.57 eV and the threshold for its dissociative ionization to form $C_5H_5^+$+H is 12.62 eV,[76] indicating that ion $C_5H_6^+$ is quite stable; about 93 kcal mol^{-1} is required to break a C–H bond of $C_5H_6^+$. If 1,3-cyclopentadiene were produced, then there

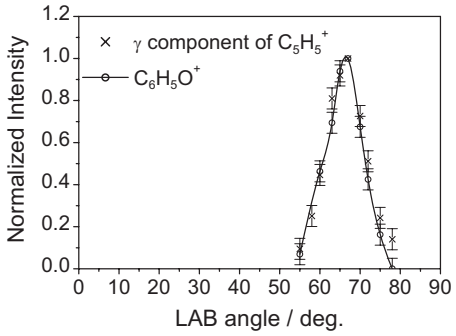

FIG. 3. Angular distributions of $C_6H_5O^+$ and the γ component of $C_5H_5^+$ [Fig. 1(f)] in the laboratory frame.

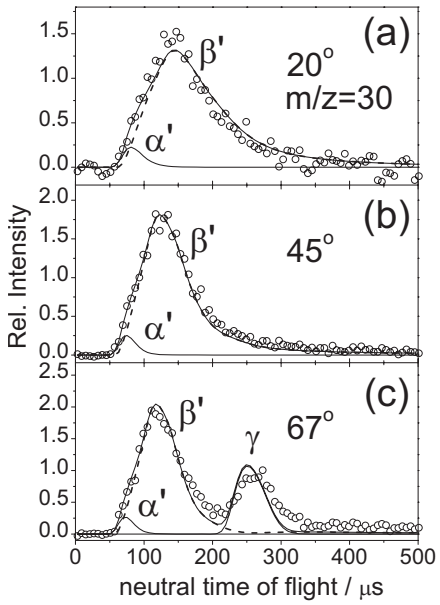

FIG. 4. Typical TOF spectra at mass 30 ($C^{18}O^+$ products) in the crossed-beam experiment of $^{18}O(^1D)+C_6H_6$ at collision energy of 10 kcal mol^{-1}. Three components α', β', and γ are discussed in text.

would be no difficulty in observing its parent ion with the electron-impact detector.[77] The fact that the proportion of $C_5H_6^+$ observed was much smaller than that of $C_5H_5^+$ suggests that channels (5b) and (6b) dominate over channel (5a).

Because the background signal of $C^{16}O$ was non-negligible, it was difficult to investigate CO product directly. Instead, we replaced the $^{16}O(^1D)$ source with $^{18}O(^1D)$ and detected directly the $C^{18}O$ product at mass 30. As shown in Fig. 4, two components, α' and β', fit the TOF spectra of the $C^{18}O$ product. The signal γ was observable only at angles near the CM angle and is attributed to a daughter ion of C_6H_5O produced from reaction (6a). The more rapid component, α', is momentum-matched to C_5H_6 (the α component) and the slow one, β', to C_5H_5+H (the β component). The $C^{18}O$ data also indicate that channels (5b) and (6b) are dominant.

Figure 5 shows the primary $P(E_T)$ used to fit reactions (5a), (5b), (6b), and (6a). The $P(E_T)$ of channels (5a), (5b), and (6b) fit satisfactorily data from both O(^1D)+C_6H_6 and O(^1D)+C_6D_6 experiments; whereas for reasons of resolution, the $P(E_T)$ of channel (6a) was determined only from the experiment of O(^1D)+C_6D_6. For the three-fragment channels (5b) and (6b), the momentum exerted by the H atom is negligible because of its small mass; we can thus analyze only the momentum-matching condition for C_5H_5 and CO. Practically high background at m/z=1 makes detection of the H product unattainable. Nevertheless, we can see from Fig. 10 that there is no reverse barrier for these H atom loss processes. Therefore, the kinetic energy of the H atom product is expected to be small. The momentum of the H atom product would be relatively minor in comparison with those of the C_5H_5 and CO products. In the analysis, we only used the two masses of C_5H_5 and CO. That is, the presented $P(E_T)$ for channels (5b) and (6b) includes only the translational energies of the C_5H_5 and CO products, with the small amount of translational energy of the H atom excluded. The

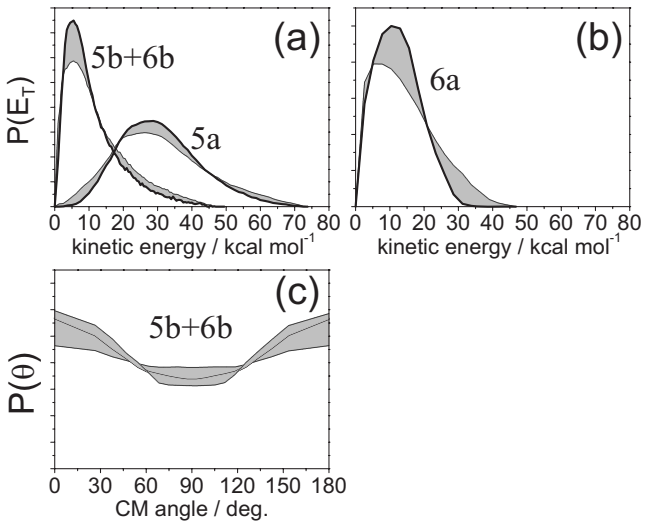

FIG. 5. (a) Kinetic-energy distribution $P(E_T)$ used to fit channels (5a) and (5b)+(6b); (b) $P(E_T)$ used to fit channel (6a); and (c) $P(\theta)$ used to fit channels (5b) and (6b). Boundaries of the shaded area indicate limits of the distributions which still give acceptable fits to the experimental data. An isotropic angular distribution was used to fit channels (5a) and (6a).

$P(\theta)$ for these channels are either isotropic or forward-backward symmetric, indicating a reaction mechanism associated with an long-lived complex.

It is difficult to investigate the channel for formation of OH from $O(^1D)+C_6H_6$ because the background signal from residual H_2O gas is large; hence, we investigated this channel in the reaction of $^{18}O(^1D)+C_6D_6$. A weak ^{18}OD signal was detected within a limited range of laboratory angles. The TOF spectrum and $P(E_T)$ are shown in Fig. 6. In these experiments, a slightly different collision energy was used to increase the intensity of the $O(^1D)$ beam. As $P(\theta)$ cannot be accurately determined from the limited data, we assumed an isotropic $P(\theta)$ in the preliminary analysis.

B. Infrared emission of CO from the flow experiments

To maintain a feasible condition as nearly collisionless as practicable, we decreased the partial pressure of O_3 and

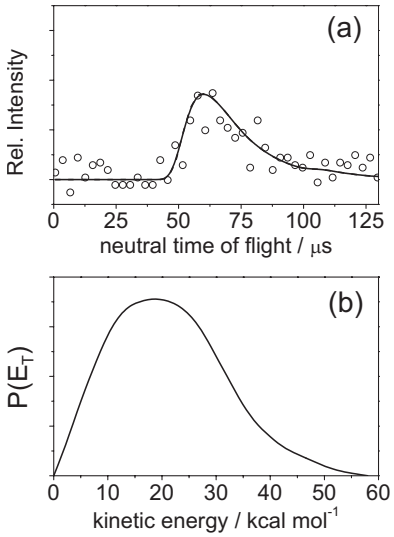

FIG. 6. (a) TOF spectra and (b) the corresponding $P(E_T)$ of OD product in crossed-beam experiments with $O(^1D)+C_6D_6$ at collision energy of 12 kcal mol^{-1}.

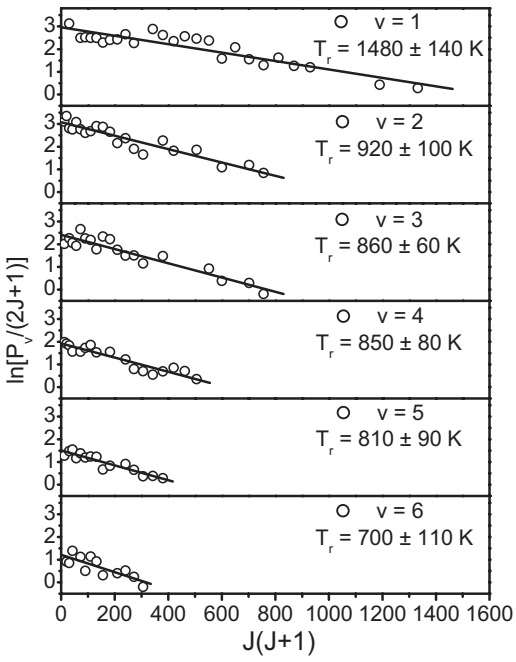

FIG. 7. Semilogarithmic plots of relative rotational populations of CO ($v=1-6$, circle) upon photolysis of a flowing mixture of O_3 (0.097 Torr) and C_6H_6 (0.020 Torr) at 248 nm. Solid lines represent least-squares fits.

C_6H_6 while maintaining a satisfactory signal to noise ratio. This ratio for the OH bands is superior to that for CO because a decreased spectral resolution was required for OH and the Einstein coefficients of OH are, in general, greater. Satisfactory spectra of CO were hence obtained on averaging six spectra that were recorded in separate experiments under similar conditions.

We assigned lines of CO based on spectral parameters reported by Ogilvie *et al.*[78] and employed values of Einstein *A* coefficients of CO calculated previously.[79,80] The spectrum exhibits emission of CO with J' up to 30 and v' up to 6. Each vibration-rotational line was normalized with the relative instrument response factors and divided by its respective Einstein coefficient to yield a relative population $P_v(J')$. Partially overlapped lines of CO, such as $J'=11,22,28$ of $v'=1$, $J'=7,12,22,25$ of $v'=2$, $J'=3,8,14,21$ of $v'=3$, and $J'=2,14,20$ of $v=4$, were deconvoluted to yield their intensities.

Semilogarithmic plots of $P_v(J')/(2J'+1)$ versus $J'(J'+1)$ for CO ($v'=1-6$) recorded 0–5 μs upon photolysis of O_3 appear in Fig. 7. Fitted Boltzmann-type rotational distributions of CO, derived from the spectrum recorded in the range of 0–5 μs, yielded rotational temperatures of 1480 ± 140, 920 ± 100, 860 ± 60, 850 ± 80, 810 ± 90, and 700 ± 110 K for $v'=1-6$, respectively; unless specified otherwise, listed error limits represent one standard deviation in fitting. An average rotational energy of $E_r=1.9\pm0.3$ kcal mol^{-1} was observed for CO ($v=1-6$). In our previous work on $O(^1D)+CO$,[79] we observed that rotational quenching of CO is non-negligible under our experimental conditions ($P_{CO}=0.058$ and $P_{O3}=0.016$ Torr) even at 5 μs; hence, we fitted the rotational temperature of CO at varied periods upon photolysis to an exponential decay and estimated the nascent rotational temperature to be

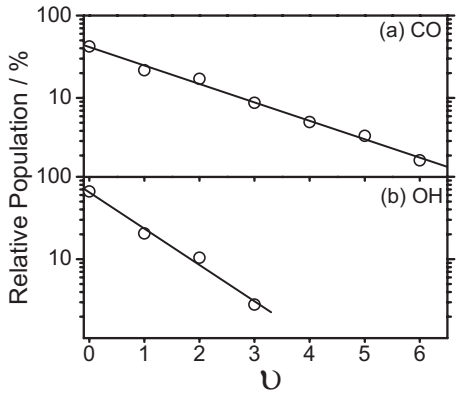

FIG. 8. Relative vibrational distributions of CO [panel (a)] and OH [panel (b)] upon photolysis of a flowing mixture of O_3 (0.097 Torr) and C_6H_6 (0.020 Torr) at 248 nm. The populations of $v=0$ are estimated from Boltzmann distributions.

1890 ± 120, 1180 ± 110, 1090 ± 90, 1040 ± 70, and 1000 ± 80 K for CO ($v=1$) to CO ($v=5$), respectively. After applying a correction factor of 1.26 for rotational quenching based on decay in the rotational temperature, we estimated a nascent rotational energy of 2.4 ± 0.4 kcal mol^{-1} based on the observed data.

We assumed a Boltzmann distribution and associated an interpolated population with overlapped lines. The relative populations obtained on counting levels up to the observed J_{max} in each vibrational level were normalized to yield a relative vibrational population $(v=1):(v=2):(v=3):(v=4):(v=5):(v=6)=37.6:29.5:15.1:8.8:5.6:3.0$, corresponding to a vibrational temperature of 5800 ± 330 K. Assuming a Boltzmann distribution, we estimated the population of $v=0$ to be 2.2 ± 0.2 times that of $v=1$. The vibrational distribution of CO normalized for $v=0-6$ is thus $(v=0):(v=1):(v=2):(v=3):(v=4):(v=5):(v=6)=45.2:20.7:17.0:8.2:4.7:2.9:1.3$, as shown in Table I and Fig. 8(a). The average vibrational energy of CO thus derived is $E_v=8.0\pm0.7$ kcal mol^{-1}. Vibrational quenching is negligible within 5 μs; the correction is less than 3%.

C. Infrared emission of OH from the flow experiments

Emission spectra of OH, at a resolution of 1.0 cm^{-1}, were recorded 0–5 μs after photolysis of O_3 (0.097 Torr) and C_6H_6 (0.020 Torr). Assignments were based on spectral parameters reported by Colin *et al.*[81] The spectrum exhibits emission from OH with values of K' up to 9 and v' up to 3. Each vibration-rotational line in the P branch was analyzed to yield a relative population $P_v(K')$, using Einstein coefficients reported by Holtzclaw *et al.*[82] Semilogarithmic plots of $P_v(K')/(2K'+1)$ versus $K'(K'+1)$ for OH ($v=1-3$) recorded 0–5 μs after photolysis of O_3 are shown in Fig. 9. There is a negligible variation in the population of OH for the two spin-orbit components. Fitted rotational distributions of Boltzmann type for the $P1$ and $P2$ branches of OH ($v'=1-3$) yield rotational temperatures of 660 ± 20, 570 ± 20 and 690 ± 40 K, as listed in Table I. An average rotational energy of $E_r=1.5\pm0.2$ kcal mol^{-1} for OH ($v=1-3$) observed 0–5 μs after photolysis is derived. Based on the derived rotational temperatures of OH

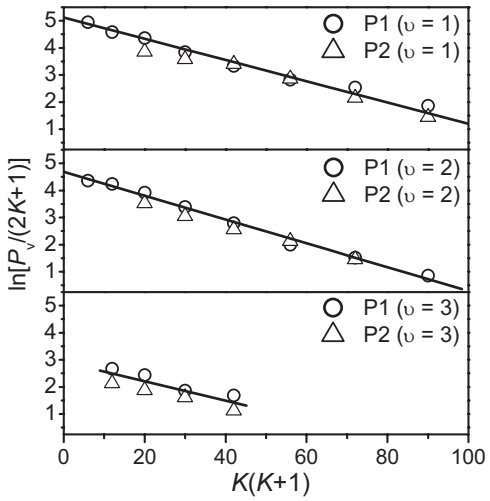

FIG. 9. Semilogarithmic plots of relative rotational populations of OH ($v=1-3$; $P1$ branch, circle; $P2$ branch, open triangle) upon photolysis of a flowing mixture of O_3 (0.097 Torr) and C_6H_6 (0.020 Torr) at 248 nm. Solid lines represent least-squares fits.

($v=1-2$) as a function of reaction periods, we estimated the average nascent rotational temperatures to be 680 ± 10 and 610 ± 10 K for OH ($v=1$) and OH ($v=2$), respectively. The nascent average rotational energy of OH is thus $E_r=1.6\pm0.3$ kcal mol^{-1}.

The relative vibrational population of OH was derived to be $(v=1):(v=2):(v=3)=60.6:30.9:8.5$, corresponding to a vibrational temperature of 4830 ± 230 K. Assuming a Boltzmann distribution, we estimated the population of $v=0$ to be 3.2 ± 0.3 times that of $v=1$. The vibrational distribution of OH normalized for $v=0-3$ is thus $(v=0):(v=1):(v=2):(v=3)=66.1:20.6:10.5:2.9$, as shown in Table I and Fig. 8(b). The average vibrational energy of OH thus derived is $E_v=5.0\pm1.0$ kcal mol^{-1}.

D. Branching ratios and their D-isotopic effect

We searched for the HCO signal in the crossed-beam experiments but detected no signal at mass 31 (HC $^{18}O^+$). Because the background at this mass is small and the HCO^+ ion is stable, any neutral HCO product, if formed, is hence detectable as HCO^+; we concluded that the channel yielding HCO is negligible.

We assumed similar detection efficiencies of C_5H_6 and C_5H_5 in the electron-impact ionization/detection and determined the branching ratio of channels (5a)/[(5b)+(6b)] by analyzing the TOF spectra of $C_5H_6^+$ and $C_5H_5^+$, together with their daughter ions down to C_5^+. Daughter ions smaller than C_5^+ are expected to have negligible contributions as the C_5-ring is quite stable. The Jacobian factor in the transformation from a laboratory frame to the CM frame is included in the analysis. For $O(^1D)+C_6H_6$ and $O(^1D)+C_6D_6$ reactions, the branching ratios of channels (5a)/[(5b)+(6b)] were determined to be 0.12 ± 0.03 and 0.13 ± 0.02, respectively. A similar procedure is applicable to channel (6a), for which the branching ratio of channels (6a)/[(5b)+(6b)] was deduced to be 0.38 ± 0.06 for the $O(^1D)+C_6D_6$ reaction. The large mass

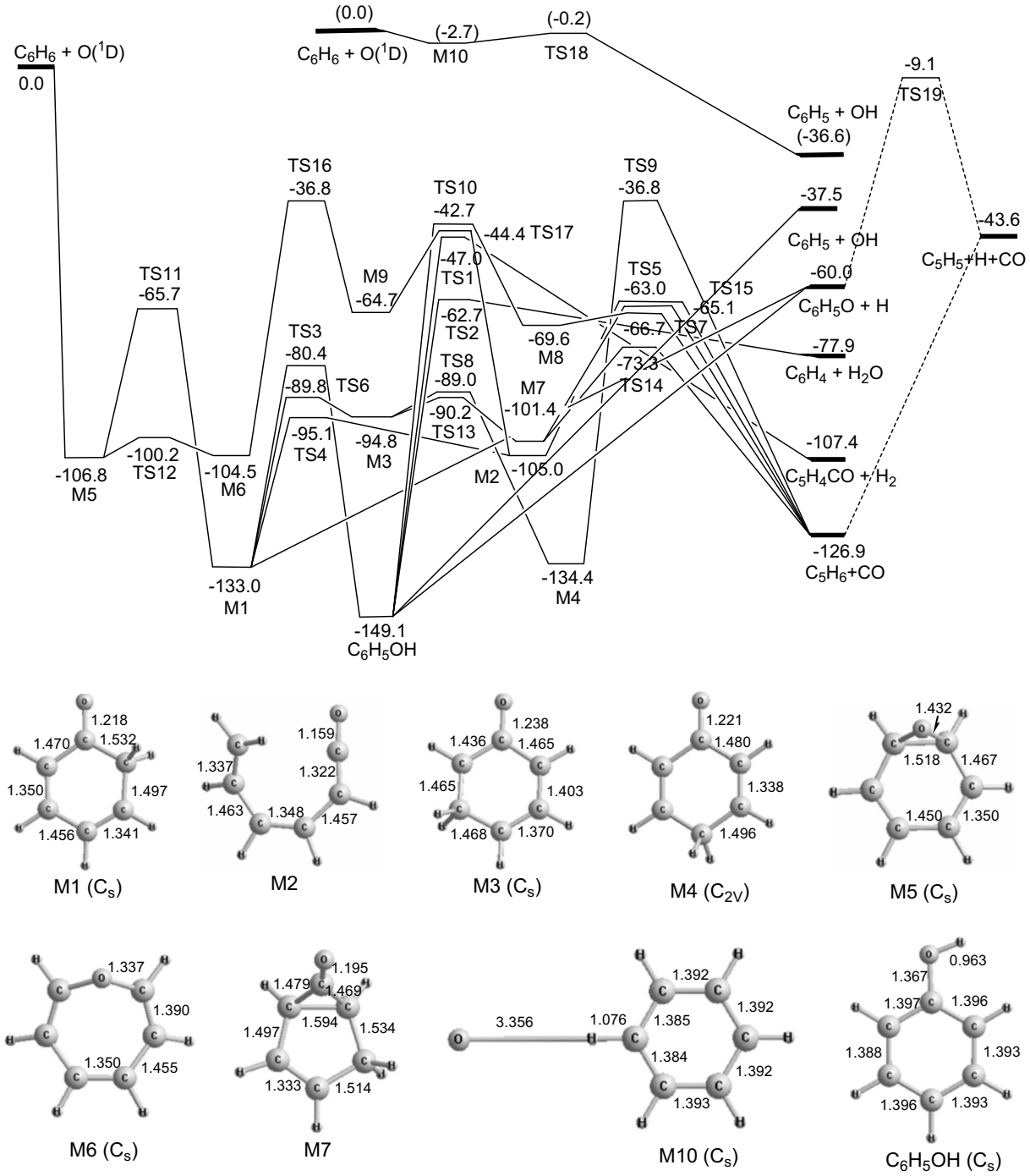

FIG. 10. Energy profile for $C_6H_6+O(^1D)$ at the G2M//B3LYP/6-311G(d,p) level for the association/isomerization/decomposition channels and at the CIPT2//CAS(8,8)/6-311G(d,p) level for the H-abstraction channel (separate line on top with ordinates shifted upward slightly and energy listed in parentheses). Energies are in kcal mol^{-1}. Structures of some key intermediates are also shown. Bond lengths are in Å.

ratio of the products limits the resolution of $P(E_T)$ for channels (6a) and (6b); the error bar of this branching ratio is consequently larger.

Only a weak ^{18}OD signal was detected from $^{18}O(^1D)+C_6D_6$ within a limited range of laboratory angles. As no OD signal was detected from the reaction with the $O(^3P)$ source from SO_2 photolysis, we can exclude the possibility that the ^{18}OD signal arises from the reaction of $^{18}O(^3P)$; we conclude that the formation of ^{18}OD is minor, with a branching ratio of <0.1.

The relative branching ratios of the channels to form CO and OH were also determined with TR-FTS on summing the total populations of the products, including estimates of $v=0$. Care was taken to correct the small background signal of OH measured when no C_6H_6 was added; the signal might result from reactions of $O(^1D)$ with background H_2O and trace hydrocarbons in the system. After correction for this interference, the ratio of [CO]/[OH] was derived to be 2.1 ± 0.2.

In the $O(^1D)+C_6D_6$ experiment, IR emission of CO but not OD was detected. The signal to noise ratio of CO emission in this experiment was ~4.2. Although accurate

TABLE I. Fitted rotational temperature T_{rot}, average rotational energy E_{rot}, and vibrational population of CO(v) and OH(v) recorded 0–5 μs upon irradiation of a flowing mixture of O_3 (0.097 Torr) and C_6H_6 (0.02 Torr) at 248 nm.

	CO			OH		
v	T_{rot} (K)	E_{rot} (kcal)	Population	T_{rot} (K)	E_{rot} (kcal)	Population
0			(0.452)[a]			(0.661)[a]
1	1480 ± 140	2.63	1.000 (0.207)	660 ± 20[b]	0.98	1.000 (0.206)
2	920 ± 100	1.63	0.785 (0.170)	570 ± 20	0.79	0.509 (0.105)
3	860 ± 60	1.43	0.402 (0.082)	690 ± 40	0.88	0.138 (0.029)
4	850 ± 80	1.17	0.234 (0.047)			
5	810 ± 90	1.10	0.160 (0.029)			
6	700 ± 110	0.69	0.080 (0.013)			

[a]Normalized population with v=0 predicted from Boltzmann distribution.
[b]Average rotational temperature for $P1$ and $P2$ branches.

Einstein coefficients of OD are unavailable, we estimated these based on the theory that they are proportional to the cube of frequency and to the square of the matrix element[83] Assuming roughly $\sqrt{2}$ as the ratio of reduced masses of OD and OH, the matrix elements for Δv=1 transitions of OH and OD have a ratio of $1/\sqrt{2}$, and the frequency factor ratio is approximately $(1/\sqrt{2})^3$. The maximal Einstein coefficient of OD is hence ~18% those of OH, which are, in turn, ~7% those of CO. The signal to noise ratio (S/N) for OH in our experiments with O(^1D)+C_6H_6 was about 15; hence, we expect that, under similar conditions, this ratio for OD in the reaction O(^1D)+C_6D_6 to be about 2.7 if the same amount of OD were produced. The fact that we observed no detectable emission of OD ($S/N<2$) indicates that there is a substantial deuterium isotopic effect with [OH]/[OD]>1.4, that is, [CO]/[OD]>2.9 in the reaction of O(^1D)+C_6D_6.

E. PES for the reaction

The predicted potential-energy diagram and some important intermediate structures are presented in Fig. 10; all symbols given in the figure are identical to those given previously for the decomposition of phenol.[43,44] New product channels characterized by M9, TS16, TS17, M10, and TS18 are added into this figure. The uncertainties of the calculated enthalpy of reaction are estimated to be about ±3 kcal mol^{-1} when we compare the calculated values with known experimental results. As the mechanism for the unimolecular decomposition of C_6H_5OH, a key intermediate in the O(^1D)+C_6H_6 reaction, has been previously discussed in detail,[43,44] our discussion of the present system focuses on the initial bimolecular processes and the isomerization of the excited intermediate to C_6H_5OH.

The geometric parameters of various new intermediates and transition states are available from the Electronic Physics Auxiliary Publication Service (EPAPS).[84] The reaction of O(^1D) with C_6H_6 can occur along two distinct paths—an addition to one C=C bond to give benzene oxide (M5) and a direct H abstraction (via TS18) to give OH and C_6H_5. Our repeated searches for the C–H insertion product C_6H_5OH always resulted in the ring-addition intermediate M5. This addition reaction to produce M5 occurs with no barrier and is exothermic by 106.8 kcal mol^{-1}. The barrierless path of minimum energy (MEP), calculated with the B3LYP/6-311G(d,p) method by manually stretching the length of bond O–C from 1.4 Å at M5 to 4.6 Å, corresponding to a structure asymptotic to the reactants, is presented well by the Morse function, $V(R_{O-C})=108.8\{1-\exp[-1.949(R_{O-C}-1.400)]\}^2$ kcal mol^{-1}, in which R_{O-C} in unit of angstroms denotes one of the two stretching O···C_6H_6 isosceles bonds. The MEP was employed to evaluate the branching ratio for production of CO relative to OH, to be discussed later.

Benzene oxide (M5) can isomerize to 2,4-cyclohexadienone (M1) or oxepin (M6) via transition states TS11 (–65.7 kcal mol^{-1} relative to the reactants) or TS12 (–100.2 kcal mol^{-1}), respectively. The latter ring-enlargement isomerization with a small barrier of 6.6 kcal mol^{-1} apparently occurs more readily. The former concerted isomerization reaction via TS11 has a large barrier because it involves both C–O bond breaking and H migration. Further isomerization from M6 to M9 is, however, more difficult than those from M1 to M2, M3, and C_6H_5OH because the energy of TS16 (–36.8 kcal mol^{-1}) is much greater than those of TS4 (–95.1 kcal mol^{-1}), TS6 (–89.8 kcal mol^{-1}), and TS3 (–80.4 kcal mol^{-1}). The dominant reaction channels are hence predicted to be the isomerization/decomposition paths through M1, as in the case of the thermal and photolytic decomposition reactions studied previously;[43,44] the reaction channel from M6 to M9 via TS16 is expected to be kinetically noncompetitive in the reaction O(^1D)+C_6H_6.

As discussed previously,[43,44] M1 can decompose to form C_5H_6+CO via two channels: one through M2 and TS5 and the other through M3, TS13, M7, and TS14. Although the barrier for M1 to form M2 via TS4 has an energy of 5.3 kcal mol^{-1} less than that for M1 to form M3 via TS6, the latter channel is predicted to be dominant because, in the product outlet, the energy of transition state TS5 is 10.3 kcal mol^{-1} greater than that of TS14. The transition state TS3 for isomerization of M1 to phenol (C_6H_5OH) has energy greater than those of TS6 and TS4 by 9.4 and 14.7 kcal mol^{-1}, respectively. Furthermore, transition states TS2 and TS1 for the decomposition channels of C_6H_5OH also have energies greater than those of transition states

TS14 and TS5. In addition to these channels, M1 might also decompose to form C_6H_5O+H via a loose variational transition state with the dissociation energy of 73.0 kcal mol^{-1}. Similarly, C_6H_5OH might decompose to form C_6H_5O+H and, to a lesser extent, C_6H_5+OH, via loose transition states. Nevertheless, to estimate the rate coefficients for production of H and OH, we computed the MEP of both $M1 \rightarrow C_6H_5O+H$ and $C_6H_5OH \rightarrow C_6H_5+OH$ at the B3LYP/6-311G(d,p) level of theory; they are described with Morse functions $V(R_{C-H})=80.4\{1-\exp[-4.68(R_{C-H}-1.35)]\}^2$ kcal mol^{-1} and $V(R_{C-O})=117.1\{1-\exp[-2.413(R_{C-O}-1.467)]\}^2$ kcal mol^{-1}, respectively. Further decomposition of C_6H_5O to C_5H_5 and CO involves a large potential barrier of 50.9 kcal mol^{-1} via a three-step isomerization, which was discussed in detail by Liu *et al.*[85] The elimination of H from C_5H_6 involves a loose transition state that is endothermic by 83.3 kcal mol^{-1}, as shown in Fig. 10. Because the fragments C_5H_6+CO+H have less energy than the reactants by 43.6 kcal mol^{-1}, this decomposition is expected to occur more readily than the decomposition of C_6H_5O.

The direct H abstraction occurs via transition state TS18 to form a hydrogen-bonded complex, $O\cdots HC_6H_5$ (M10). These structures were optimized with various methods, BH&HLYP, MP2, and CAS(8,8) (Ref. 86) using the 6-311G(d,p) basis set. The B3LYP method failed to locate either M10 or TS18, which is predicted to have C_s symmetry with an imaginary wavenumber of 730i cm^{-1} at BH&HLYP, 1989i cm^{-1} at MP2, and 4789i cm^{-1} at CAS(8,8). In TS18, the breaking C−H bond is predicted to have lengths of 1.18, 1.23, and 1.21 Å, and the evolving O−H bond to have lengths of 1.22, 1.24, and 1.28 Å, respectively, at the BH&HLYP, MP2, and CAS(8,8) levels. In M10, the $O\cdots HC_6H_5$ bond is predicted to have a length of 2.80 Å at the BH&HLYP level and 3.06 Å at the CAS(8,8) level. These critical geometric parameters are similar to those of the hydrogen-abstraction channel in the reaction of $O(^1D)+C_2H_6$ reported by Sun *et al.*[28] The energies of M10 and TS18 have been refined by the CIPT2 method[87] based on the geometric parameters optimized at the CAS(8,8)/6-311G(d,p) level. To evaluate the energy relative to the reactants, we calculated the energy of the supermolecule ($O\cdots HC_6H_5$) with a separation of 25 Å between the two fragments, C_6H_6 and $O(^1D)$. The results show that M10 and TS18 lie at −2.7 and −0.2 kcal mol^{-1}, respectively, relative to the reactants at the CIPT2 level. At the same level of theory, another supermolecule ($OH\cdots C_6H_5$) with the separation of 25 Å between two radicals C_6H_5 and OH, approximately considered to be the C_6H_5+OH products, was calculated to lie at −36.6 kcal mol^{-1}, 0.9 kcal mol^{-1} less than that calculated with the G2M method. These results were employed for calculations of the relative product yields of the reaction of $O(^1D)+C_6H_6$. Reaction (7) is insufficiently exothermic for secondary dissociation to occur; as predicted at the G2M level, $C_6H_5 \rightarrow H+C_6H_4$ requires an activation energy of 77 kcal mol^{-1}.

V. DISCUSSION

A. Reaction channels and thermal rate coefficients

For the channel to form CO from the thermal decomposition of C_6H_5OH, the rate coefficients determined with a flow tube[88] and a shock tube[89] are quantitatively accounted for with the following paths:[43]

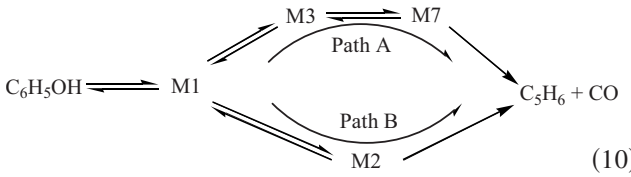

(10)

The dynamics of formation of CO in the photofragmentation of C_6H_5OH at 248 or 193 nm is consistent with this mechanism.[44] In the photofragmentation of C_6H_5OH, additional product channels producing C_6H_5O+H and H_2O (at 193 nm only) were detected.

The reaction of $O(^1D)+C_6H_6$ is expected to occur primarily via routes of two types: (1) a low-energy path via M1, followed by isomerization/decomposition to produce C_5H_6+CO, C_6H_5O+H, and C_6H_5+OH, and (2) an abstraction path via M10 to produce C_6H_5+OH.

$$O(^1D) + C_6H_6 \leftrightarrow M5^* \leftrightarrow M1^* \rightarrow C_6H_5O + H \quad (11a)$$

$$\leftrightarrow C_6H_5OH^* \rightarrow C_6H_5 + OH \quad (11b)$$

$$\leftrightarrow M2^* \rightarrow C_5H_6 + CO \quad (11c)$$

$$\leftrightarrow M3^* \leftrightarrow M7^* \rightarrow C_5H_6 + CO \quad (11d)$$

$$C_6H_6 + O(^1D) \leftrightarrow M10 \rightarrow C_6H_5 + OH. \quad (12)$$

As discussed in Sec. IV E, the major channel for production of OH is the direct abstraction [reaction (12)], rather than the addition/decomposition in reaction (11b). For the formation of CO via channels (11c) and (11d), the latter is dominant because the energy of TS14 is predicted to be less than that of TS5 by 9.7 kcal mol^{-1}; at 300 K, $k_{(11d)}$ is about five to six times $k_{(11c)}$, whereas at 1400 K, the ratio decreases to 2.

The rate coefficients for various channels under low-pressure conditions were calculated with the RRKM theory and variational transition-state theory with the VARIFLEX code of Klippenstein *et al.*[64] The pressure dependence of the individual and total thermal rate coefficients for the formation of CO, H, and OH at 300 K over diverse pressures using He as a bath gas are shown in Fig. 11. The total rate coefficient is independent of pressure below 1000 atm. The individual rate coefficients k(CO), k(H), and k(OH), in which the reaction product is shown in parentheses, remain nearly constant under pressures less than ~600 Torr; experimental conditions in this work are thus at the low-pressure limit.

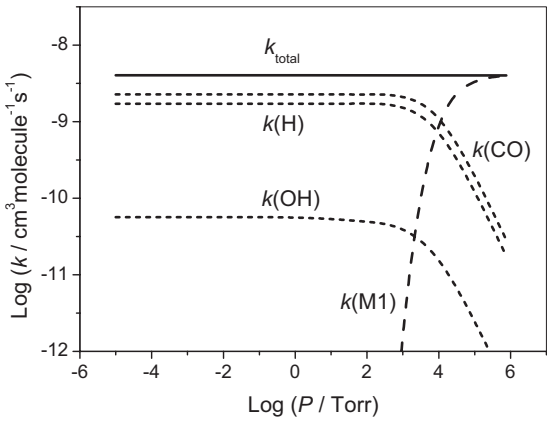

FIG. 11. Total and individual thermal rate coefficients for the reaction O(^1D)+C_6H_6 as a function of pressure at 300 K.

Figure 12(a) shows the temperature dependence of the individual and total thermal rate coefficients at the low-pressure limit in the temperature range of 200–2000 K. The total rate coefficient exhibits a small positive temperature dependence and is expressed as

$$k(\text{total}) = 2.42 \times 10^{-9} T^{0.1.08} \exp(-23/T) \quad \text{cm}^3 \text{ molecule}^{-1} \text{ s}^{-1}. \tag{13}$$

The total thermal rate coefficient is mainly contributed by those for formation of CO and H,

$$k(\text{CO}) = 4.37 \times 10^{-9} T^{-0.087} \exp(19/T) \quad \text{cm}^3 \text{ molecule}^{-1} \text{ s}^{-1} \quad (T = 200 - 500 \text{ K}), \tag{14a}$$

$$k(\text{CO}) = 5.67 \times 10^{-12} T^{0.924} \exp(-504/T) \quad \text{cm}^3 \text{ molecule}^{-1} \text{ s}^{-1} \quad (T = 500 - 2000 \text{ K}), \tag{14b}$$

$$k(\text{H}) = 3.76 \times 10^{-8} T^{-0.383} \exp(12/T) \quad \text{cm}^3 \text{ molecule}^{-1} \text{ s}^{-1}, \tag{15}$$

respectively. The rate coefficient for formation of k(OH), including both decomposition [reaction (11b)] and abstraction [reaction (12)] channels,

$$k(\text{OH}) = 5.78 \times 10^{-6} T^{-1.47} \exp(163/T) \quad \text{cm}^3 \text{ molecule}^{-1} \text{ s}^{-1} \tag{16}$$

is about one-tenth that of k(CO) and k(H). k(M1) makes a negligible contribution to the total rate coefficient under our experimental conditions. Individual branching ratios are given in Fig. 12(b). As the temperature increases, the yield of CO decreases whereas that of H increases; the branching ratio of OH remains small even at high temperatures.

B. Channels to produce CO

As multistep isomerization is required to form CO, a protracted duration and an approximately statistical distribution of energy are expected, consistent with the experimental observations. CO was observed in the crossed-molecular-beam experiment to be a major product, but the expected

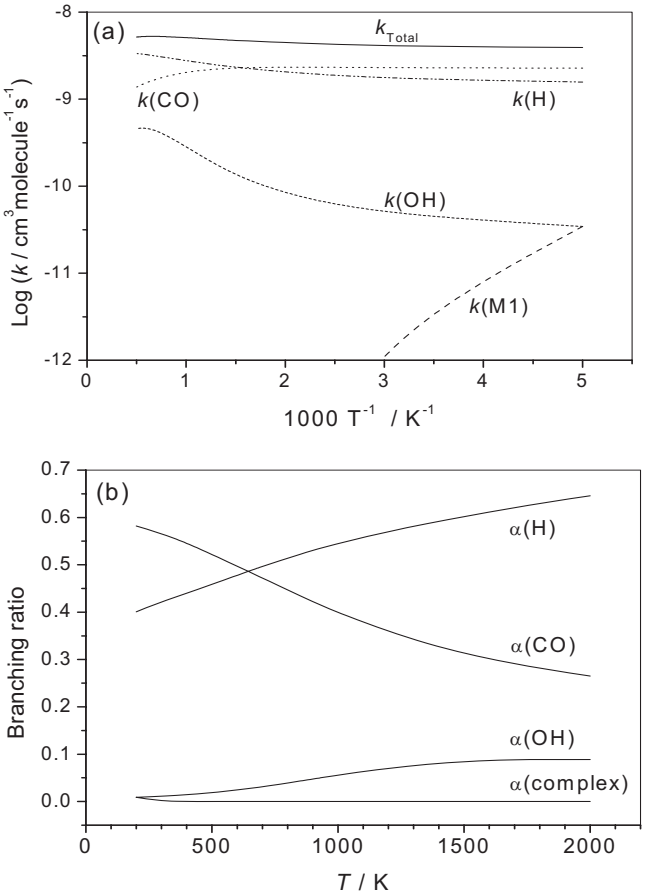

FIG. 12. (a) Total and individual thermal rate coefficients for the reaction O(^{1}D)+C_6H_6 as a function of temperature at the low-pressure limit. (b) Individual branching ratio as a function of temperature at the low-pressure limit.

counterproduct C_5H_6 tends to decompose further to C_5H_5+H [reaction (5b)]. Similarly, some C_6H_5O produced with internal energy exceeding the dissociation barrier (for TS 19) might decompose further to C_5H_5 and CO [reaction (6b)]. The three-fragment channel, C_5H_5+CO+H, is exothermic by 43.6 kcal mol^{-1}, but there is a barrier for the secondary process $C_6H_5O^* \rightarrow C_5H_5$+CO. For channel (6a), the primary H product carries no internal energy and the primary translational energy release is expected to be small because there is no reverse barrier for the formation of C_6H_5O+H. At this point, it is difficult to estimate the branching ratio between reactions (5b) and (6b) from these experiments.

In TR-FTS experiments, nascent rotational temperatures of 1890 ± 120, 1180 ± 110, 1090 ± 90, 1040 ± 70, and 1000 ± 80 K for CO (v=1) to CO (v=5) were derived; the rotational temperature of CO (v=1) appears to be greater than the rotational temperatures of CO (v=2–5). One possibility is that CO produced from reaction (6b) is populated only at v=0 and 1 because of the smaller exothermicity and large barrier; the greater rotational temperature for CO produced in this channel might be related to the geometry of the transition state. The torque angle of TS19 (~56°) is much larger than that of TS14 (~13°); it is therefore expected that the CO produced from channel (6b) would have a greater rotational excitation than that from channels (5a) and (5b),

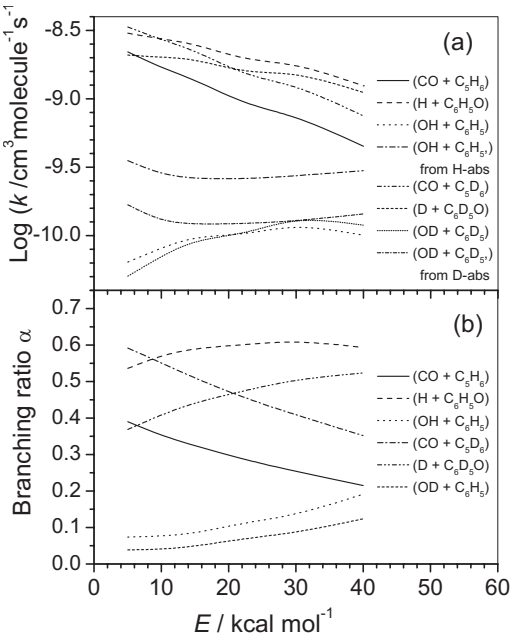

FIG. 13. (a) Individual product microcanonical rate coefficients of the reaction $O(^1D)+C_6H_6$ as a function of energy. (b) Individual product microcanonical branching ratios as a function of energy.

whereas that from channels (5a) and (5b) would have a less rotational excitation but a greater vibrational excitation.

In the photolysis of phenol at 193 nm, the available energy of 148 kcal mol^{-1} above C_6H_5OH is near that of the reaction $O(^1D)+C_6H_6$, 149+10=159 kcal mol^{-1}; the kinetic energy of $O(^1D)$, produced upon photolysis of O_3 at 248 nm, with respect to the CM for $O(^1D)+C_6H_6$ was reported to be 10.2 kcal mol^{-1}.[90] Previous experiments on photolysis of phenol at 193 nm indicated a nascent rotational temperature of ~4600 K for CO (v=1–4) and an observed vibrational distribution of (v=1):(v=2):(v=3):(v=4) =64.3:22.2:9.1:4.4 corresponding to a vibrational temperature of 3350±20 K; an average rotational energy of 6.9±0.7 kcal mol[1] and vibrational energy of 3.8±0.7 kcal mol^{-1} were derived.[44] In the present work on $O(^1D)+C_6H_6$, the CO product shows less rotational excitation (2.4±0.4 kcal mol^{-1}) but greater vibrational excitation (8.0±0.7 kcal mol^{-1}). A separate phase space might be sampled for these two photolytic and bimolecular processes, even though they might be expected to proceed across the same PES.

C. Channels to produce OH

Most OH is produced via a direct abstraction; the behavior from a single channel is expected. In TR-FTS experiments, nascent rotational temperatures of OH were determined to be 680±10 and 610±10 K for OH (v=1–2), respectively.

The O–H bond length in transition state TS18 is 1.279 Å, and the angle C–H–O is almost linear. The small torque angle in the transition state implies little rotational excitation of OH, consistent with our observation of average rotational energy of only 1.6±0.3 kcal mol^{-1}. The O–H bond length in TS18, which is much elongated relative to the value of 0.97 Å for diatomic OH, indicates that the OH product might be highly vibrationally excited, consistent with our observation of population of OH up to v=3 with a vibrational energy of ~29 kcal mol^{-1}. The observed average vibrational energy of OH, 5.0±1.0 kcal mol^{-1}, is 10.7% of the total available energy. This fraction is large if one considers the complexity of the counterproduct C_6H_5.

D. Branching ratios and D-isotopic effect

The microcanonical rate coefficients k and the branching ratios α for the formation of various products are shown in Fig. 13(a), with $k_H(E)>k_{CO}(E)>k_{OH\text{-}(12)}(E)>k_{OH\text{-}(11b)}(E)$; the latter two correspond to the formation of OH via reactions (11b) and (12), respectively. These rate coefficients take no account of secondary dissociation channels. Reactions (11c) and (11d) hence correspond to reactions (5a) and (5b), reaction (11a) corresponds to reactions (6a) and (6b), whereas reactions (11b) and (12) correspond to reaction (7).

As the excitation energy of the $O(^1D)+C_6H_6$ reaction increases from 5 to 40 kcal mol^{-1}, the branching ratio α(H) increases slightly from 0.54 to 0.60, α(OH) increases from 0.07 to 0.19, whereas α(CO) decreases from 0.39 to 0.21, as indicated in Fig. 13(b). The reaction system $O(^1D)+C_6D_6$ shows a substantial deuterium kinetic isotopic effect; $k_{CO}(E)$ and $k_{OH}(E)$ increase whereas $k_H(E)$ becomes smaller upon deuteration of C_6H_6.

In the beam experiments, the observed branching ratio for production of OD from $O(^1D)+C_6D_6$ is less than 0.1, consistent with the predicted branching ratio 0.04 at E=10 kcal mol^{-1} [Fig. 13(b)]. Because of secondary decompositions, it is difficult to make a direct comparison between the calculated and experimental branching ratios for the H and CO channels.

As the energy increases from 5 to 40 kcal mol^{-1}, $k_{CO}(E)/k_{OH}(E)$ decreases from 5.27 to 1.13 and $k_{CO}(E)/k_{OD}(E)$ decreases from 15.37 to 2.85; the ratios for the reaction of $O(^1D)+C_6D_6$ are 2.9–2.5 times greater than those for $O(^1D)+C_6H_6$. At an energy of 10.2 kcal mol^{-1}, the kinetic energy of $O(^1D)$ with respect to the CM upon photolysis of O_3 at 248 nm, α(CO):α(OH)=0.35:0.08=4.3, agrees qualitatively with the experimental value of α(CO)/α(OH)=2.1±0.2 determined with TR-FTS. Some observed CO might be produced via reaction (6b), involving secondary dissociation of C_6H_5O but the proportion is expected to be small, and likely a major part has been taken into account in performing the extrapolation of the populations to CO (v=0).

For the reaction of $O(^1D)+C_6D_6$, the ratio α(CO):α(OD) is predicted to be 0.55:0.04 at an energy of 10.2 kcal mol^{-1}; the ratio of α(CO)/α(OD) is ~2.9 times that of α(CO)/α(OH) in the reaction of $O(^1D)+C_6H_6$. Our experimental observation of an isotopic ratio α(OH)/α(OD)>1.4 is consistent with this result. According to our calculations, the ratio $k_{OH}(E)/k_{OD}(E)$ for the hydrogen abstraction is predicted to be about 2.1 in the energy range from 5 to 40 kcal mol^{-1}, as expected from the deuterium isotopic effect.

VI. CONCLUSION

The reaction between $O(^1D)$ and C_6H_6 was investigated with crossed-molecular-beam reactive scattering and time-resolved Fourier-transform infrared emission experiments. The mechanism of the reaction may be understood by considering the energetics of the intermediate species and transition states calculated at the G2M(CC5) level of theory for the PES of the $O(^1D)+C_6H_6$ reaction. The major channel is the formation of the three fragments $CO+C_5H_5+H$; channels for formation of C_5H_6+CO, C_6H_5O+H, and $OH+C_6H_5$ are minor. The angular distributions for formation of CO and H indicate a mechanism involving a long-lived collision complex. The CO product from the C_5H_6+CO channel might have much vibrational but little rotational excitation, whereas that from the secondary decomposition of C_6H_5O might populate up to only $v=1$ with greater rotational excitation. The small rotational excitation for the OH ($v\leq 3$) product and the deuterium isotopic effect is consistent with a H-abstraction mechanism rather than insertion, followed by scission of the CO bond. Based on infrared emission experiments, the branching ratio of [CO]/[OH] is $\sim 2.1\pm 0.4$ for $O(^1D)+C_6H_6$ and [CO]/[OD] is greater than 2.9 for the $O(^1D)+C_6D_6$ reaction. From molecular-beam experiments the branching ratios of [CO+stable C_5H_6]/[CO from the three-fragment channel] $=0.12\pm 0.03$ and [D+stable C_6H_5O]/[D from the three-fragment channel] $=0.38\pm 0.06$ are derived. Because of the limitation of each method, absolute values of the branching ratios cannot be derived, but the relative values are consistent with theoretical predictions.

ACKNOWLEDGMENTS

The National Science Council of Taiwan supported this work under Contract Nos. NSC96-2113-M009-025 and NSC95-2113-M-001-041-MY3. Z.F.X. acknowledges a partial support from the Basic Energy Science, Department of Energy under Contract No. DE-FG02-97-ER14784. M.C.L. is grateful to the National Science Council of Taiwan for a Distinguished Visiting Professorship and to Taiwan Semiconductor Manufacturing Co. for a TSMC Distinguished Professorship at National Chiao Tung University, Taiwan.

[1] K. Mikulecky and K.-H. Gericke, J. Chem. Phys. **96**, 7490 (1992).
[2] C. B. Cleveland, G. M. Jursich, M. Tolier, and J. R. Wiesenfeld, J. Chem. Phys. **86**, 3253 (1987).
[3] P. M. Aker and J. J. Sloan, J. Chem. Phys. **85**, 1412 (1986).
[4] D. G. Sauder, J. C. Stephenson, D. S. King, and M. P. Casassa, J. Chem. Phys. **97**, 952 (1992).
[5] D. S. King, D. G. Sauder, and M. P. Casassa, J. Chem. Phys. **97**, 5919 (1992).
[6] C. B. Cleveland and J. R. Wiesenfeld, J. Chem. Phys. **96**, 248 (1992).
[7] F. J. Comes, K.-H. Gericke, and J. Manz, J. Chem. Phys. **75**, 2853 (1981).
[8] J. E. Butler, L. D. Talley, G. K. Smith, and M. C. Lin, J. Chem. Phys. **74**, 4501 (1981).
[9] S. G. Cheskis, A. A. Iogansen, P. V. Kulakov, I. Yu. Razuvaev, O. M. Sarkisov, and A. A. Titov, Chem. Phys. Lett. **155**, 37 (1989).
[10] J. Schlutter, R. Schott, and K. Kleinermanns, Chem. Phys. Lett. **213**, 262 (1993).
[11] M. Brouard, H. M. Lambert, J. Short, and J. P. Simons, J. Phys. Chem. **99**, 13571 (1995).
[12] J. J. Lin, Y. T. Lee, and X. Yang, J. Chem. Phys. **109**, 2975 (1998).
[13] F. Ausfelder, H. Hippler, and F. Striebel, Z. Phys. Chem. **214**, 403 (2000).
[14] R. Sayos, J. Hernando, M. P. Puyuelo, P. A. Enriquez, and M. Gonzalez, Phys. Chem. Chem. Phys. **4**, 288 (2002).
[15] P. M. Aker, J. J. A. O'Brien, and J. J. Sloan, J. Chem. Phys. **84**, 745 (1986).
[16] J. Shu, J. J. Lin, Y. T. Lee, and X. Yang, J. Chem. Phys. **114**, 4 (2001).
[17] J. Shu, J. J. Lin, C. C. Wang, Y. T. Lee, X. Yang, T. L. Nguyen, and A. M. Mebel, J. Chem. Phys. **115**, 7 (2001).
[18] C. C. Wang, J. Shu, J. J. Lin, Y. T. Lee, X. Yang, T. L. Nguyen, and A. M. Mebel, J. Chem. Phys. **116**, 8292 (2002).
[19] X. Yang, Phys. Chem. Chem. Phys. **8**, 205 (2006).
[20] T. J. Dillon, A. Horowitz, and J. N. Crowley, Chem. Phys. Lett. **443**, 12 (2007).
[21] A. C. Luntz, J. Chem. Phys. **73**, 1143 (1980).
[22] C. R. Park and J. R. Wiesenfeld, J. Chem. Phys. **95**, 8166 (1991).
[23] M. Gonzalez, M. P. Puyuelo, J. Hernando, R. Sayos, P. A. Enriquez, J. Guallar, and I. Banos, J. Phys. Chem. A **104**, 521 (2000).
[24] J. P. Simons, J. Chem. Soc., Faraday Trans. **93**, 4095 (1997).
[25] A. J. Alexander, M. Brouard, K. S. Kalogerakis, and J. P. Simons, Chem. Soc. Rev. **27**, 405 (1998).
[26] H. Tsurumaki, Y. Fujimura, and O. Kajimoto, Chem. Phys. Lett. **301**, 145 (1999).
[27] A. H. H. Chang and S. H. Lin, Chem. Phys. Lett. **363**, 175 (2002).
[28] Y. C. Sun, I. T. Wang, T. L. Nguyen, H. F. Lu, X. Yang, and A. M. Mebel, J. Phys. Chem. A **107**, 6986 (2003).
[29] A. H. H. Chang and S. H. Lin, Chem. Phys. Lett. **384**, 229 (2004).
[30] H. G. Yu and J. T. Muckerman, J. Phys. Chem. A **108**, 8615 (2004).
[31] S. Sato and R. J. Cvetanović, Can. J. Chem. **36**, 1668 (1958).
[32] O. Kajimoto and T. Fueno, Chem. Phys. Lett. **64**, 445 (1979).
[33] O. Kajimoto, H. Yamasaki, and T. Fueno, Chem. Phys. Lett. **68**, 127 (1979).
[34] K. Honma, J. Chem. Phys. **99**, 7677 (1993).
[35] M. Gonzalez, M. P. Puyuelo, J. Hernando, R. Sayos, R. Sayos, and P. A. Enriquez, Chem. Phys. Lett. **346**, 69 (2001).
[36] S. J. Sibener, R. J. Buss, P. Casavecchia, T. Hirooka, and Y. T. Lee, J. Chem. Phys. **72**, 4341 (1980).
[37] T. M. Sloane, J. Chem. Phys. **67**, 2267 (1977).
[38] N. J. Barry, I. W. Fletcher, and J. C. Whitehead, J. Phys. Chem. **90**, 4911 (1986).
[39] J. M. Nicovich, C. A. Gump, and A. R. Ravlshankara, J. Phys. Chem. **86**, 1684 (1982).
[40] T. Ko, G. Y. Adusei, and A. Fontijn, J. Chem. Phys. **95**, 8745 (1991).
[41] D. Hodgson, H. Y. Zhang, M. R. Nimlos, and J. T. McKinnon, J. Phys. Chem. A **105**, 4316 (2001).
[42] T. L. Nguyen, J. Peeters, and L. Vereecken, J. Phys. Chem. A **111**, 3836 (2007).
[43] Z. F. Xu and M. C. Lin, J. Phys. Chem. A **110**, 1672 (2006).
[44] C. M. Tseng, Y. T. Lee, M. F. Lin, C. K. Ni, S. Y. Liu, Y. P. Lee, Z. F. Xu, and M. C. Lin, J. Phys. Chem. A **111**, 9463 (2007).
[45] S.-R. Lin, S.-C. Lin, Y.-C. Lee, Y.-C. Chou, I.-C. Chen, and Y.-P. Lee, J. Chem. Phys. **114**, 160 (2001).
[46] S.-R. Lin, S.-C. Lin, Y.-C. Lee, Y.-C. Chou, I.-C. Chen, and Y.-P. Lee, J. Chem. Phys. **114**, 7396 (2001).
[47] M. J. Perri, A. L. Van Wyngarden, K. A. Boering, J. J. Lin, and Y. T. Lee, J. Phys. Chem. A **108**, 7995 (2004).
[48] J. J. Lin, D. W. Hwang, Y. T. Lee, and X. Yang, J. Chem. Phys. **109**, 1758 (1998).
[49] T. L. Nguyen, A. M. Mebel, and S. H. Lin, J. Chem. Phys. **114**, 1758 (2001).
[50] T. Berndt and O. Boge, Z. Phys. Chem. **218**, 391 (2004).
[51] M. Brouard, R. Cireasa, A. P. Clark, T. J. Preston, C. Vallance, G. C. Groenenboom, and O. S. Vasyutinskii, J. Phys. Chem. A **108**, 7965 (2004).
[52] U. Even, J. Jortner, D. Noy, N. Lavie, and C. Cossart-Magos, J. Chem. Phys. **112**, 8068 (2000).
[53] R. K. Sparks, K. Shobatake, L. R. Carlson, and Y. T. Lee, J. Chem. Phys. **75**, 3838 (1981); R. I. Kaiser, C. Ochsenfeld, D. Stranges, M. Head-Gordon, and Y. T. Lee, Faraday Discuss. **109**, 183 (1998).
[54] C. Y. Wu, C. Y. Chung, Y. C. Lee, and Y. P. Lee, J. Chem. Phys. **117**, 9785 (2002).
[55] P. S. Yeh, G. H. Leu, Y. P. Lee, and I. C. Chen, J. Chem. Phys. **103**, 4879 (1995).
[56] S. R. Lin and Y. P. Lee, J. Chem. Phys. **111**, 9233 (1999).

[57] S. K. Yang, S. Y. Liu, H. F. Chen, and Y. P. Lee, J. Chem. Phys. **123**, 224304 (2005).
[58] Y. Matsumi and M. Kawasaki, Chem. Rev. (Washington, D.C.) **103**, 4767 (2003).
[59] W. B. DeMore and O. Raper, J. Phys. Chem. **68**, 412 (1964).
[60] A. M. Mebel, K. Morokuma, and M. C. Lin, J. Chem. Phys. **103**, 7414 (1995).
[61] M. J. Frisch, G. W. Trucks, H. B. Schlegel *et al.*, GAUSSIAN 03, Revision C.02, Gaussian, Inc., Wallingford CT, 2004.
[62] A. D. Becke, J. Chem. Phys. **98**, 5648 (1993); **96**, 2155 (1992).
[63] C. Lee, W. Yang, and R. G. Parr, Phys. Rev. B **37**, 785 (1988).
[64] S. J. Klippenstein, A. F. Wagner, R. C. Dunbar, D. M. Wardlaw, and S. H. Robertson, VARIFLEX, Version 1.00. 1999.
[65] W. L. Hase, J. Chem. Phys. **57**, 730 (1972).
[66] W. L. Hase, Acc. Chem. Res. **16**, 258 (1983).
[67] D. M. Wardlaw and R. A. Marcus, Chem. Phys. Lett. **110**, 230 (1984).
[68] D. M. Wardlaw and R. A. Marcus, J. Chem. Phys. **83**, 3462 (1985).
[69] S. J. Klippenstein and R. A. Marcus, J. Chem. Phys. **87**, 3410 (1987).
[70] S. J. Klippenstein, J. Chem. Phys. **96**, 367 (1992).
[71] C. Eckart, Phys. Rev. **35**, 1303 (1931).
[72] W. H. Miller, J. Chem. Phys. **65**, 2216 (1976).
[73] D. C. Astholz, J. Troe, and W. Wieters, J. Chem. Phys. **70**, 5107 (1979).
[74] D. C. Tardy and B. S. Rabinovitch, J. Chem. Phys. **45**, 3720 (1966).
[75] F. M. Mourits and F. H. A. Rummens, Can. J. Chem. **55**, 3007 (1977).
[76] J. L. Occolowitz and G. L. White, Aust. J. Chem. **21**, 997 (1968).
[77] S. E. Stein, NIST Mass Spectrometry Data Center, in *NIST Chemistry Web Book*, NIST Standard Reference Database No. 69, edited by P. J. Linstrom and W. G. Mallard (National Institute of Standards and Technology, Gaithersburg MD, 2005), http://webbook.nist.gov
[78] J. F. Ogilvie, S. L. Cheah, Y. P. Lee, and S. P. A. Sauer, Theor. Chem. Acc. **108**, 85 (2002).
[79] H. F. Chen and Y. P. Lee, J. Phys. Chem. A **110**, 12096 (2006).
[80] C. Y. Wu, Y. P. Lee, J. F. Ogilvie, and N. S. Wang, J. Phys. Chem. A **107**, 2389 (2003).
[81] R. Colin, P. F. Coheur, M. Kiseleva, A. C. Vandaele, and P. F. Bernath, J. Mol. Spectrosc. **214**, 225 (2002).
[82] K. W. Holtzclaw, J. C. Person, and B. D. Green, J. Quant. Spectrosc. Radiat. Transf. **49**, 223 (1993).
[83] J. F. Ogilvie, *The Vibrational and Rotational Spectroscopy of Diatomic Molecules* (Academic, London, UK, 1998).
[84] See EPAPS Document No. E-JCPSA6-129-018839 for geometries, rotational and vibrational parameters of various intermediates and transition structures. For more information on EPAPS, see http://www.aip.org/pubservs/epaps.html.
[85] R. Liu, K. Morokuma, A. M. Mebel, and M. C. Lin, J. Phys. Chem. **100**, 9314 (1996).
[86] M. J. Frisch, I. N. Ragazos, M. A. Robb, and H. B. Schlegel, Chem. Phys. Lett. **189**, 524 (1992).
[87] P. Celani, H. Stoll, and H.-J. Werner, Mol. Phys. **102**, 2369 (2004).
[88] A. B. Lovell, K. Brezinsky, and I. Glassman, Int. J. Chem. Kinet. **21**, 547 (1989).
[89] C. Horn, K. Roy, P. Frank, and T. Just, Proceedings of the 27th Symposium International on Combustion, 1998 (unpublished), Vol. 321.
[90] M. Abe, Y. Inagaki, L. L. Springsteen, Y. Matsumi, M. Kawasaki, and H. Tachikawa, J. Chem. Phys. **98**, 12641 (1994).